Additive Manufacturing Letters 9 (2024) 100194

Contents lists available at ScienceDirect

Additive Manufacturing Letters

journal homepage: www.elsevier.com/locate/addlet

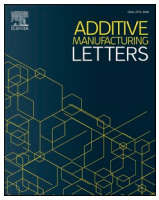

Short Communication

Effect of Process Parameters in Additively Manufactured Sensors prepared via Material Extrusion Processes: Correlation among Electrical, Mechanical and Microstructure Properties

Gianni Stano, Neshat Sayah, Douglas E. Smith, Trevor J. Fleck *

Department of Mechanical Engineering, Baylor University, 1 Bear Place #97356, Waco, TX 76798

ARTICLE INFO

Keywords:
Material Extrusion Additive Manufacturing
Microstructure
Sensors
Process Parameters

ABSTRACT

Fusion-based Material Extrusion (MEX) Additive Manufacturing (AM) processes have been extensively used for the fabrication of smart structures with embedded sensors, proving to have several benefits such as reduction in cost, manufacturing time, and assembly. A major issue negatively affecting 3D printed sensors is related to their poor electrical conductivity, as well as inconsistent electrical performance, which leads to electrical power losses amongst other issues. In the present paper, a set of process parameters (ironing, printing temperature, and infill overlap) has been analyzed by performing a Design of Experiment (DoE) factorial plan to minimize the electrical resistance. The best process parameters configuration involves a remarkable reduction of electrical resistance of 47.9%, as well as an improvement of mechanical properties of 31.9% (ultimate tensile strength), 25.8% (elongation at break) and 28.14% (flexural stress). The microstructure of the obtained results has also been analyzed by employing a high-resolution, X-ray Computed Tomography (X-Ray CT) system showing a reduction of intralayer voids of 19.5%. This work demonstrates a clear correlation between process parameters and the corresponding electrical properties, mechanical properties, and internal microstructure. In the present research, it has been shown that i) it is possible to significantly improve the overall 3D printed sensors performance by process parameter selection, and ii) small changes in the microstructure lead to remarkable improvements in electrical and mechanical performance.

1. Introduction

The Material Extrusion (MEX) process, defined by ISO/ASTM 52900 as the process in which materials are selectively dispensed through a nozzle or orifice, has been extensively used for the extrusion of conductive materials in order to manufacture electrical sensors [1,2] that can be easily embedded into dielectric structure during the MEX process [3]. However, the widely seen issues pertaining to quality and repeatability of mechanical performance seen in MEX samples [4], also translate to unpredictable performance issues in electrical sensors manufactured using MEX processes. A clear understanding of material-process-structure-function relationships pertaining to MEX sensors is the key enabler to improve the manufacturing process reliability, making additively manufactured sensors more appealing for industrial applications.

Besides the recent interest in capacitive-based sensors, [5–9], MEX techniques are mostly used for the fabrication of piezoresistive-based sensors. Several sensors have been 3D printed demonstrating the many benefits, as well as manufacturing flexibility, offered by MEX-technologies. In 2021, Kim et al [10] developed a multi-axial sensor by using dual extrusion with a custom-made filament, composed of a plastic matrix of polylactic acid (PLA) doped with multi wallet carbon nanotubes (MWCNTs), and a commercial thermoplastic polyurethane (TPU). The resultant piezoresistive sensors were integrated into shoes and gloves to measure the applied force when walking, jumping and lifting objects. Gronborg et al [11], in 2022, studied various geometries of strain gauges manufactured via MEX, finding an optimal geometry improving the signal amplitude by a factor of 28, which demonstrated how geometrical design variables impact on the flexural sensors performance. Emon et al [12] developed a new strategy to extrude conductive material over curved substrates to manufacture force sensors, which paved the way for increased usage of MEX processes to create smart free-form prosthetic devices. Alsharari et al [13] leveraged the multi-material MEX technique to extrude water-soluble

* Corresponding Author:
E-mail address: trevor_fleck@baylor.edu (T.J. Fleck).

https://doi.org/10.1016/j.addlet.2024.100194
Received 28 March 2023; Received in revised form 20 December 2023; Accepted 10 January 2024
Available online 20 January 2024

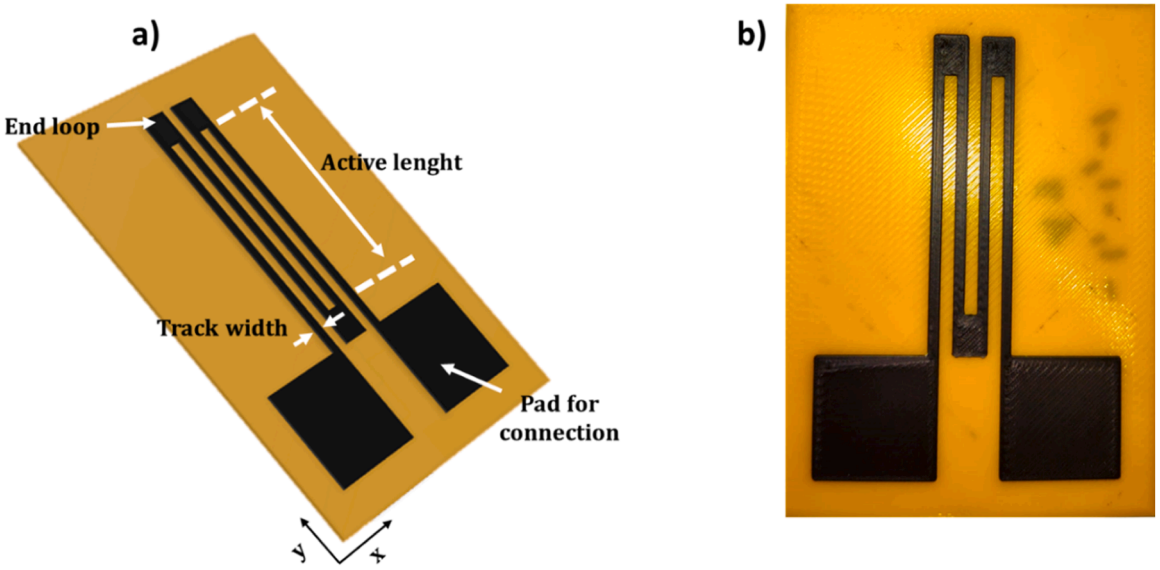

Fig. 1. Proposed sample: a) CAD design, and b) representative 3D printed sample

polyvinyl alcohol (PVA) and conductive TPU in the same printing cycle, in order to fabricate a porous multi-layered piezoresistive force/pressure sensor. The proposed sensor was characterized by a gauge factor (GF) of 6.5 at 200k Pa.

In the past few years, MEX technology has developed to encompass the fabrication of additively manufactured accelerometers [14,15,16], based on the piezoresistive effect. The possibility to fabricate, in a single step, polymer-based systems with embedded accelerometers to collect data during their usage while avoiding an assembly task, leads to a reduction in time and cost from both a manufacturing and assembly standpoint. Several theoretical and experimental studies, focused on the i) modelling of the anisotropic electrical conductivity [17], ii) dynamic behavior of the piezo resistivity[18], and iii) electrical contact mechanisms [19], iv) development of new extrudable high-conductive materials[20], are reducing the gap in knowledge about MEX-based sensors, making them more widespread and appealing for several fields.

As shown in [21], the key enabler to additively manufacturing electrical sensors via MEX processes is the extrusion and deposition of conductive polymers. Generally, a polymeric matrix is used, which is doped with conductive fillers with wt% above the percolation threshold, making the composite material conductive in accordance with the percolation theory [22]. Five types of conductive fillers are used in conductive filaments: i) carbon nanotubes (CN), ii) graphene/graphite, iii) carbon black (CB), iv) metallic fillers, and v) hybrid (combination of 2 or more fillers). One of the major issues related to conductive filaments is the high electrical resistance (low conductivity) compared to traditional conductive materials (i.e. metal) which could potentially lead to i) unwanted electrical losses due to high resistivity and the Joule effect, and ultimately ii) the impossibility to connect 3D printed sensors in a Wheatstone bridge configuration to obtain voltage-based measurements (used in load cells) . Several efforts have been made to reduce electrical resistance in MEX-based sensors. Cardenas et al [23] developed the flash ablation metallization post-processing technique based on the usage of an high intense pulsed light to vaporize the top polymeric substrate of the sensor, reducing the electrical resistance by two orders of magnitude. Another post-processing technique which proved to reduce the electrical resistance is electroless plating, based on the copper nucleation from the conductive filler within the conductive filament [24]. Additionally, there have been several process parameters of interest that have been correlated to a reduction in electrical resistance, such as raster width, air gaps, nozzle temperature, layer height and printing orientation [25–30].

Table 1
Design variables for CPLA Sensor

Variable	Value
Substrate thickness	0.4 mm
Substrate dimension in x-y	(48 – 65) mm
Sensor thickness	0.4 mm
Track width	1.2 mm
Space between two adjacent tracks	1.8 mm
Active length	30 mm
Pad dimension in x-y	(15-15) mm
End loop dimension in x-y	(4.2 – 5) mm
Number of tracks	4

The work presented in this article explores an additional set of process parameters composed of ironing, printing temperature, and infill overlap, seeking to further develop material-process-structure-function relationships for MEX sesnors. A DoE technique was used to obtain a reduction in resistance in MEX-based strain gauge sensors of 47.9%, with ironing having the highest contribution (standardized effect of 25). The proposed set of process parameters was also proved to improve mechanical properties (ultimate tensile strength, elongation at break and flexural stress of 31.9%, 25.8% and 28.14%), which is crucial to the application of these sensors as they undergo tension and compression during their usage. Microstructures of the printed sensors have been also analyzed using a high-resolution X-Ray computed tomography (X-Ray CT) system: the intra-layer voids have been reduced by 19.54%. Measurements and evaluations of the printed sensors provide new insight into the relationship between process parameters, the internal microstructure (void content) and functional performance.

2. Materials and methods

The ultimate goal of this work is to improve the electrical conductivity of fusion-based MEX sensors through finding optimal process parameters. As part of this work, the authors also seek to establish which aspects of the resultant microstructure are affected during processing and establish how these aspects map to functional performance. A multi-material Material extrusion (MEX) 3D printer was employed (Ultimaker S5, Ultimaker, Netherlands) to print two materials: a conductive polylactic acid (PLA) filament (CPLA, ProtoPasta, USA) and a neat PLA filament (PLA, Ultimaker, Netherlands). CPLA is comprised of a PLA matrix doped with carbon black (21 %wt), resulting in a conductive

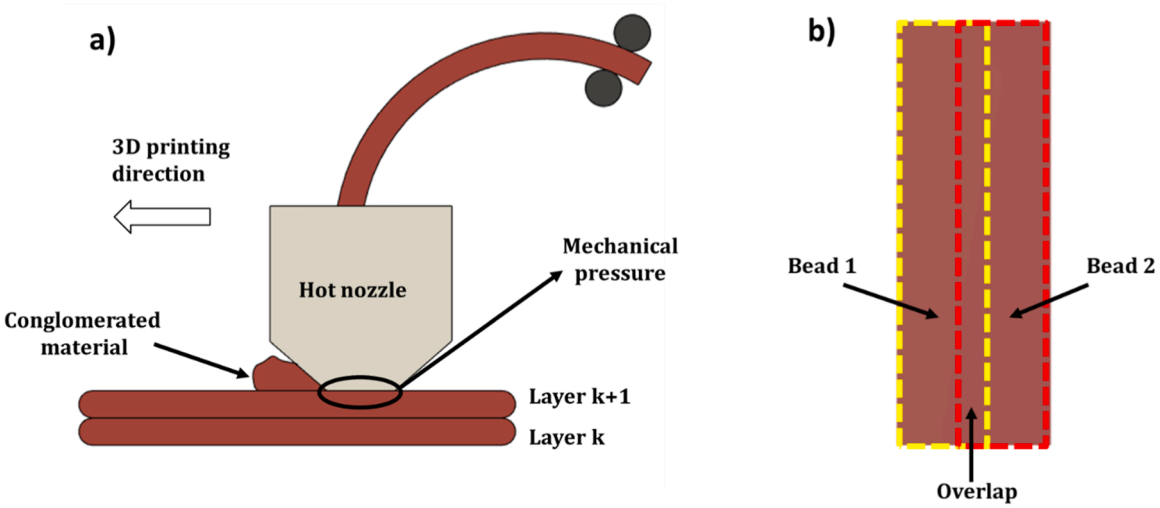

Fig. 2. Process parameters varied throughout the DoE: a) ironing parameter and b) infill overlap (top view)

polymer filament in accordance with percolation theory [22]. The CPLA material was extruded to fabricate strain gauges over a 0.4 mm thick substrate of PLA, providing a solid dielectric base. A 0.4 mm nozzle was employed for both materials. The sensor sample is shown in Fig. 1, and the design variables relevant to this work appear in Table 1.

2.1. Design of Experiment (DoE) for Electrical Resistance Minimization

A factorial plan 2^3 was performed to correlate the effect of three process parameters to the electrical resistance of 3D printed sensors. For every process parameter two levels have been investigated: level -1 (low level) and level +1 (high level). The three process parameters studied are:

- Printing Temperature: the temperature at which the nozzle is set while extruding the material. Level -1 equal to 215 ℃ (printing temperature suggested from the filament manufacture) and level +1 equal to 250 ℃ (highest temperature observed to provide a consistent extrusion). The low level -1 is representative of standard printing conditions, while the high value +1 (maximum printing temperature giving consistent extrusion) is the temperature that should be set to minimize voids, according to scientific literature [31, 32].
- Ironing: this process parameters repeats the last extruded layer by passing the hot nozzle over it and applying mechanical pressure in conjunction with heat in an effort to smooth the surface. Generally, a small amount of material (flow between 0 to 10 %) is extruded during the ironing process. Recent research correlated this parameter to surface roughness, surface morphology and thermomechanical behavior [33–35]. In the present research level -1 was set equal to ironing OFF (disabled) and level +1 equal to ironing ON (enabled). When enabled, the following set of parameters was chosen: pattern equal to zig-zag, line spacing equal to 0.05 mm, flow equal to 7% and ironing distance from the edge equal to 0.2 mm. The low level (-1) is representative of traditional printing conditions when ironing is not applied, while the high level (+1) refers to the exploitation of ironing over the last extruded layer, as shown in [34]
- Infill overlap: This parameter refers to the overlap between two adjacently extruded beads. The low level -1 was set equal to 0 mm and the high +1 level equal to 0.2 mm. The low level -1 is representative of traditional printing conditions when no overlap is used, while the high level +1 was selected by creating an overlap (0.2 mm) which is half of the width of the extruded bead (0.4 mm).

Table 2
Design of Experiment (DoE) levels and factors

	-1	+1
Printing Temperature (°C)	215	250
Ironing	OFF	ON
Infill overlap (mm)	0	0.2

Table 3
Pertinent process parameter left unchanged throughout the DoE

Variable	Value
Printing speed	25 *mm/s*
Numbers of walls	0
Layer height	0.2 mm
Line width	0.4 mm
Retraction distance	4 mm
Build plate temperature	50 ℃

The main idea underlying the selection of printing temperature, ironing and infill overlap as process parameters to be investigated is based on their effect on the layer-by-layer adhesion, as an improved adhesion could lead to a more compact structure which in turn, translates to a smoother path for the electrical current and improved electrical conductivity. Despite printing temperature and infill overlap have been proved to affect, respectively, intra-, and inter-layer adhesion[31, 36,37], the ironing process results to be still underexploited in this field. Due to its intrinsic feature of applying mechanical pressure by means of the hot nozzle, this effort investigates the effect of ironing in layer adhesion and void reduction.

An overview of the ironing and infill overlap parameters is given in Fig. 2, while the levels and factors are listed in Table 2. The pertinent process parameters used for the CPLA material, which were kept unchanged throughout the DoE, are listed in Table 3. Of note, the layer height is half the sensor thickness, meaning that only two consecutive extruded layers will be required to manufacture the sensor [25].

The DoE performed here included a number of repetitions for each level combination equal to 3 to account for variability. Printed test samples (i.e., those printed for each combination) were manufactured following a random order (generated by Minitab) to reduce the effect of uncontrollable external factors related to the manufacturing process such as vibrations, change in room temperature, humidity, etc. A total of 24 samples were fabricated.

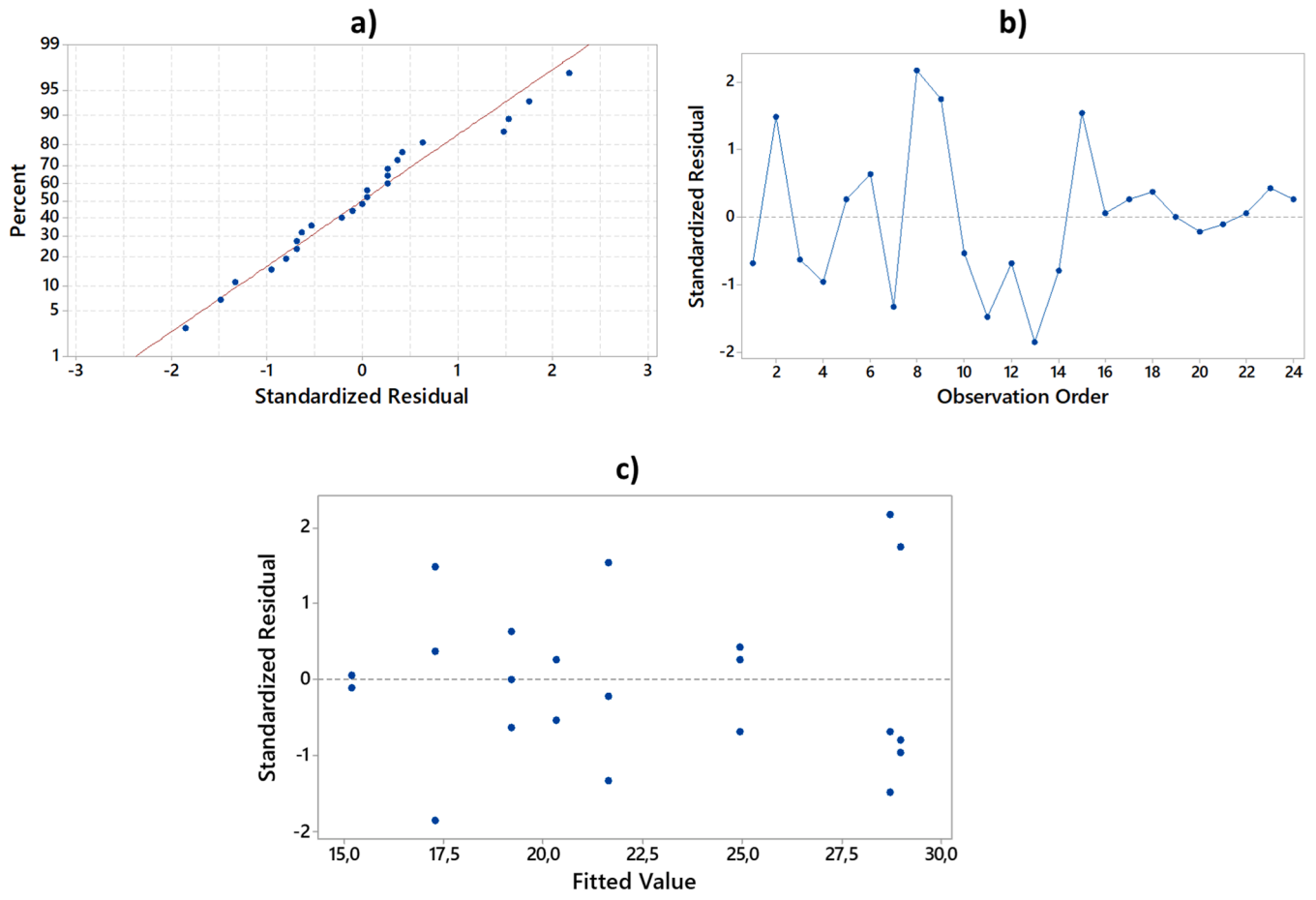

Fig. 3. DoE residuals analysis plotting (a) normal probability, (b) residual vs order, and residual vs fitted values.

2.2. Mechanical properties

Once the DoE was completed, mechanical testing was performed on CPLA samples which were fabricated using the process parameters corresponding to the highest and lowest electrical resistances. Two sets of mechanical tests were performed; tensile testing in accordance with ASTM D638 and 3-point flexural testing in accordance with ASTM D790. These two specific mechanical tests where chosen as they were representative of the application, in which strain gauges undergo both compression and tension during their lifespan. Three samples for both combination of parameters, lowest and highest electrical resistance, hereafter referred to as Batch A and B respectively, were fabricated for every mechanical test.

2.3. Microstructure Analysis via X-Ray CT

The microstructure of CPLA samples fabricated from the process parameters with lowest and highest electrical resistance were investigated using X-Ray CT. The X-Ray CT scans were performed using an NSI X3000 system (North Star Imaging, Rogers, MN, USA). In this study, the X-ray source with an acceleration voltage of 60 kV and a power of 3.5 W was used to provide adequate beam intensity and contrast in the images. Each sample was rotated 360 degrees at increments of 2 degrees during the scan, resulting in 1440 projections. The detector captured the transmitted X-ray beam signals and collected the 2D attenuation distribution image at each scan angle. All generated images had a voxel size resolution of 10 microns. The raw data from CT scans were then reconstructed into virtual 2D slices using efX-CT software (North Star Imaging, Minnesota, USA). The reconstructed data was then imported into VGStudio Max 3.4 (Volume Graphics GmbH, Heidelberg, Germany) for surface determination and void analysis. In this study, the VGDefX algorithm within the VGStudio Max porosity analysis module was used to evaluate the voxel data set for voids within the microstructure of the CPLA parts [38].

3. Results and Discussion

3.1. Results of DoE for Electrical Resistance Minimization

The goal of the DoE was to determine a combination of process parameters which minimize the electrical resistance of additively manufactured strain gauges employing CPLA. The electrical resistance of the proposed sensors was measured using a benchtop multimeter (Agilent 3410A). Particular attention was paid to the electrical contact, in which, as shown in [18], a silver paste layer was manually deposited over the pads and a copper adhesive with soldered wires was attached to minimize the contact electrical resistance due to the interaction between pads and benchtop multimeter alligator clips. The residuals analyzed in the DoE appear in Fig. 3 which indicate that the performed DoE is consistent (normal probability, and residuals vs order and fitted value), and that it has not been affected neither from the manufacturing order nor from other uncontrollable external factors.

The primary outcome of the DoE may be summarized as:

- The three parameters investigated produce a remarkable effect on the minimization of the resistance: in particular, changing values of all the three parameters from the low level (-1) to the high level (+1) resulted in a significant reduction of the electrical resistance

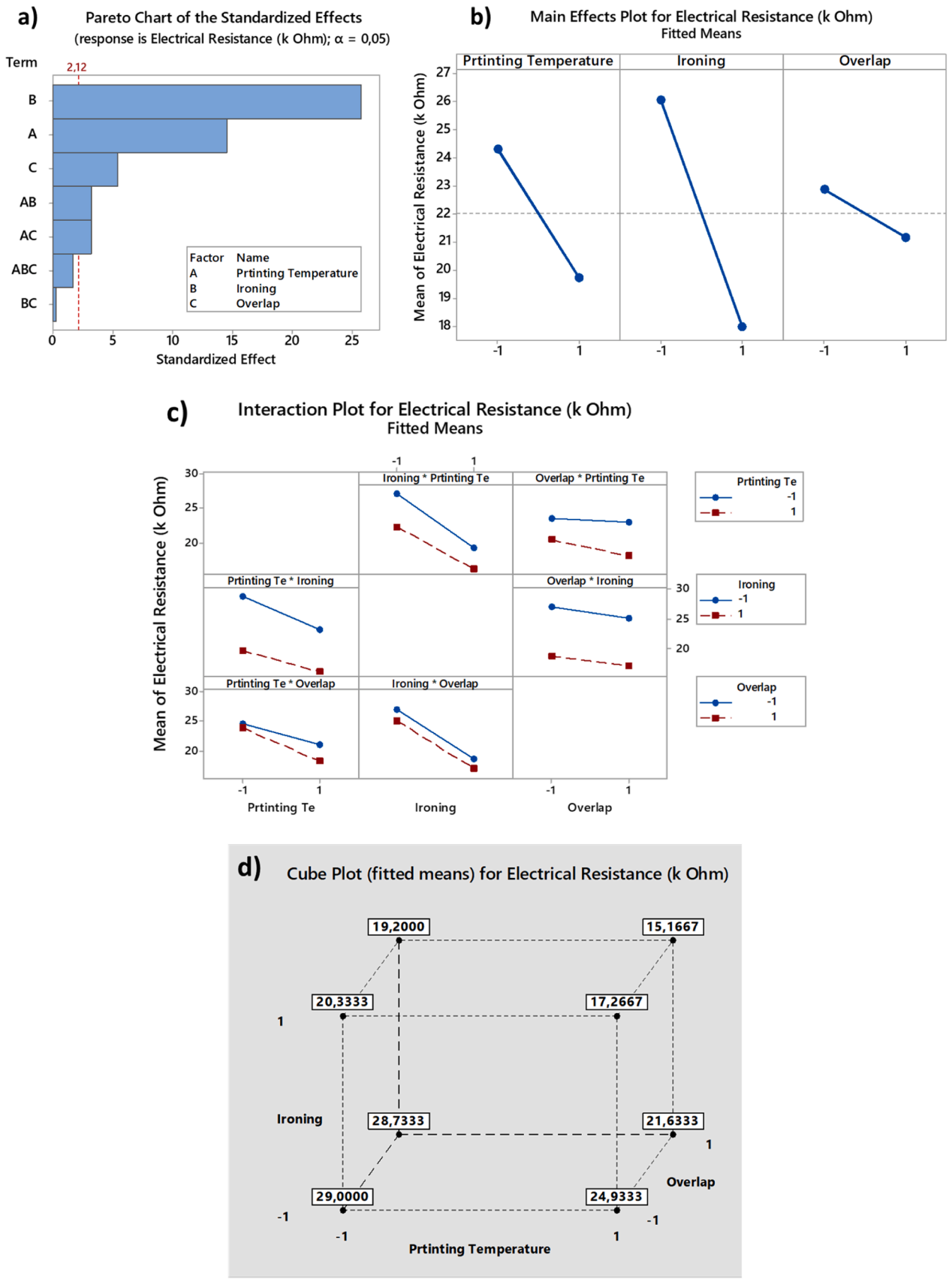

Fig. 4. DoE results- a) Standardized effect of the factors, b) main effect of the three process parameters studied, c) interaction plot of the effects, and d) cube plot

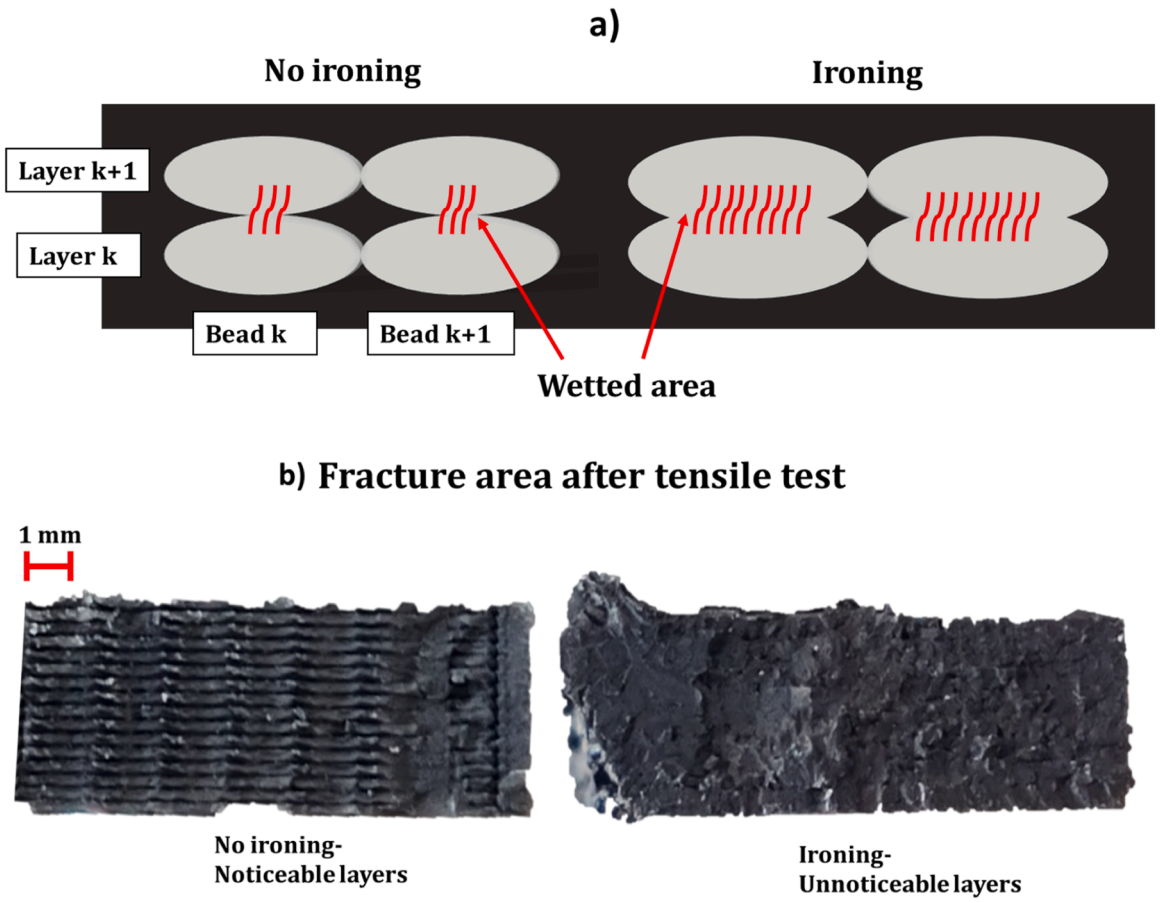

Fig. 5. a) Effect of ironing on the polymer healing process at the interface, and d) fracture face after the tensile test on additively manufactured samples

- The ironing parameters produces the highest effect (25- standardized effect), followed by the printing temperature (15- standardize effect) and infill overlap (7- standardized effect).
- The interaction between printing temperature and ironing, and printing temperature and infill overlap generates the same standardized effect of 2.8, slightly above the threshold effect of 2.12. Alternatively, the interaction between ironing and infill overlap as well as the interaction among all the three parameters does not produce any significant effect.

Details of the results discussed above appear in Fig 4. The combination of process parameters resulting in a minimal electrical resistance consists of ironing equal to +1 (ON), printing temperature equal to +1 (250°C) and infill overlap equal to +1 (0.2 mm). Employing this set of input values yielded reduced the electrical resistance by 47.9% from a mean value of 29.1 kΩ to a mean value of 15.12 kΩ The electrical resistance standard deviation, which was calculated on the three manufactured samples for each combination, was reduced from 0.9 kΩ to 0.004 kΩ when considering the lowest and highest resistance samples respectively. These findings are significant in that, the improvement of conductivity in 3D printed sensors will improve, in turn, the ability of MEX technology to fabricate structures with integrated strain gauges. The reduction of electrical resistance also involves a reduction of electrical power losses and decreased Joule effect. The final significant result observed was a reduction of standard deviation when considering the process parameters resulting in the lowest electrical resistance. When considering the application of using these sensors in a Wheatstone bridge configuration, the ability to produce sensors with a consistent, repeatable electrical resistance values is of utmost importance.

It is anticipated that the reduction in electrical resistance, as well as reduction in its standard deviation, can be attributed to a decrease in intra-layer and inter-layer voids, which has been demonstrated in similar studies [25,30]. Fig. 5(a) illustrates the effect that ironing can have on the polymer healing process at the interfaces in MEX components. Many studies have applied traditional polymer weld theory to the MEX process [39,40,41,4]. For example, Coogan et. al. [40,41] evaluated the bond strength (or interlayer adhesion (σ) in MEX components by adapting polymer reptation theory equation (equation (1)) developed in 1981 by Wool and O'Conner [39]:

$$\frac{\sigma}{\sigma_\infty} = \left[\frac{\sigma_0}{\sigma_\infty} + \frac{K}{\sigma_\infty}\, t^{\frac{1}{4}}\psi(t)\right]\phi(t) \tag{1}$$

to simulate the interlayer adhesion (σ_{sim}) as it relates to bulk material strength (σ_∞) [40] in MEX components via the following equation (2):

$$\sigma_{sim} = f_{walls} f_{wetting}\left[\sigma_0 + (\sigma_\infty - \sigma_0)\left(\frac{D_{pre}}{D_{\max}}\right)^{\frac{1}{4}}\right] \tag{2}$$

in which the $f_{wetting}$ term represents the ratio of the inter-bead connection, as shown in Fig. 5a) and 5 b), and the $\frac{D_{pre}}{D_{\max}}$ term represents the amount of polymer chain diffusion across the layer interface. Other variables include in these equations include: (t) time, ($\phi(t)$) wetting delay function, ($\psi(t)$) diffusion delay term, (K) a diffusion constant, (f_{walls}) a term used to represent the geometry of the deposition, and (σ_0), the developed strength due to wetting. The parameters of ironing, overlap, and temperature were all intentionally selected for this study, as they are known to affect the microstructure of MEX components, particularly connected area between layers, or $f_{wetting}$, as well as amount of interlayer polymer chain diffusion. The following work in Section 3.2 and 3.3 also lend credence to this hypothesis and provide explanation

Table 4
Best and Worst process parameters investigated for the minimization of electrical resistance.

	Best parameters (resistance minimization)	Worst parameters (resistance minimization)
Printing Temperature (°C)	250	215
Infill overlap (mm)	0.2	0
Ironing	Enabled	Disabled

for why the overall electrical resistance would be lowered, as well as the standard deviation; tying the correlation between less internal porosity, better mechanical performance, and the resultant reduction in electrical resistance, as well as more repeatable electrical performance.

For the reader convenience, the best and worst process parameters for the electrical resistance minimization are listed in Table X

3.2. Mechanical Tests Results

The sets of process parameters resulting in the lowest and highest electrical resistances were used to fabricate CPLA samples for mechanical testing, seeking to correlate process parameters and mechanical properties. The tests described in Section 2.2 (tensile test and 3 point flexural test) were chosen as they represent the mechanical performance of these materials in their final application. Two batches of samples for every test were fabricated: Batch A (three samples fabricated with the process parameters that resulted in the lowest (or best) electrical resistance values), and Batch B (three samples were fabricated with the process parameters which resulted in the highest (or worst) electrical resistance values). The best and worst process parameters, used respectively for the fabrication of samples belonging to Batch A and Batch B are listed in Table 4.

The samples belonging to both Batch A and Batch B were manufactured by using the other process parameters described in Table 3. In these samples, the number of walls was set to zero and the extruded beads were deposited parallel to the direction of the tensile force

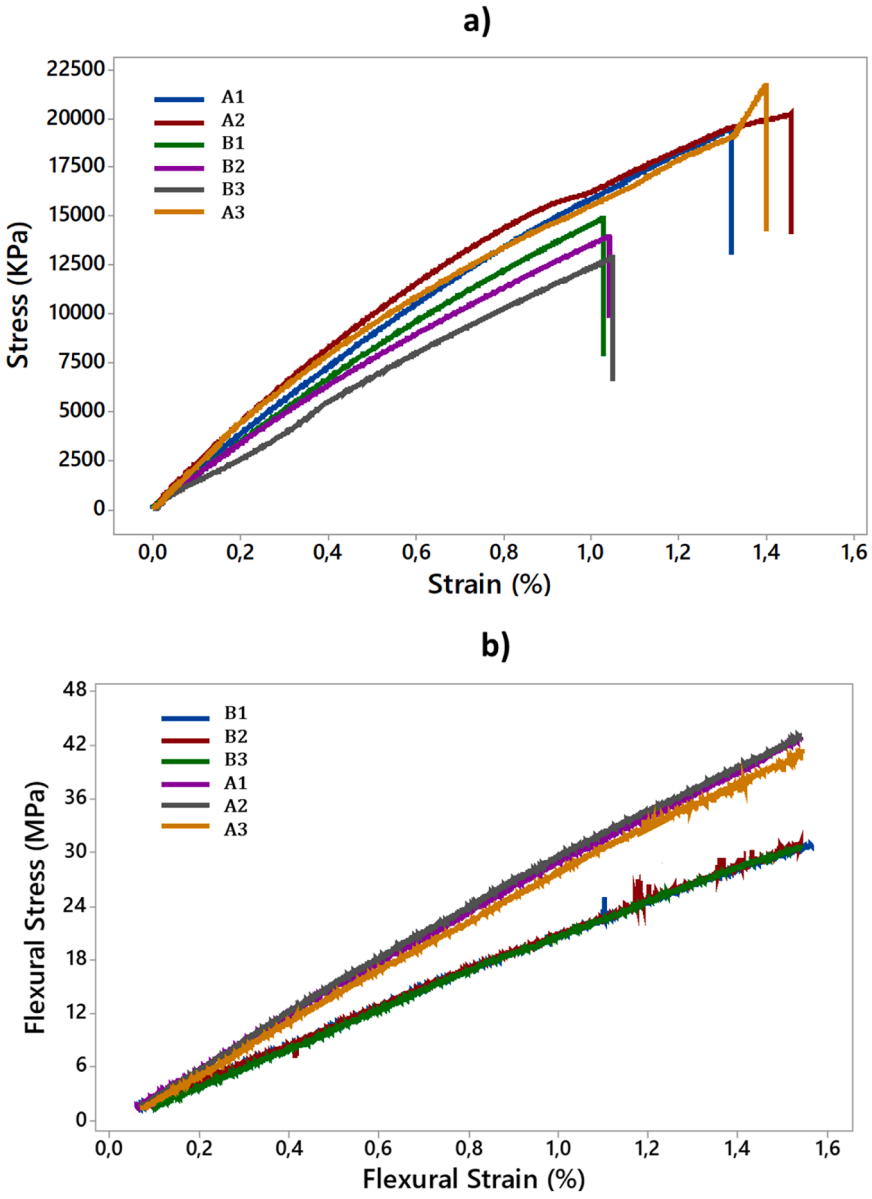

Fig. 6. Mechanical tests results for batch A and B (three repetitions for every batch): a) tensile test, b) 3 point flexural test overlap among the three curves representing B1, B2, and B3).

Table 5
Results obtained during the mechanical characterization

	Batch A	Batch B
Mean UTS	20.528 MPa	13.941 MPa-
Standard Deviation	0.967 MPa	0.795 MPa
Mean Tensile Strain at Failure	1.39%	1.03%
Standard Deviation	0.05%	0.008%
Mean Flexural Stress at Failure	41.25 MPa	26.64 MPa
Standard Deviation	1.47 MPa	1.2 MPa

Table 6
Void volume fraction

Set of parameters	Mean	Standard Deviation
Process Parameters for Lowest Electrical Resistance	4.57%	0.807
Process Parameters for Highest Electrical Resistance	5.68%	0.423

application. The number of walls were set to zero to isolate the parameters of interest to this study since it has been shown that wall (or shell) count can significantly affect the overall mechanical performance [42].

For all the samples belonging to Batch A, the ironing process parameters was used for every layer such that after extruding layer k, ironing was performed prior to depositing layer k+1, as shown in Fig. 2. The results of the tensile test and 3-point flexural test are shown in Fig 6. In test cases, the usage of the best set of process parameters (minimizing electrical resistance) resulted in a significant improvement in mechanical properties. The mean UTS and elongation at break for samples belonging to Batch A were increased by 31.9 % and 25.89%, respectively, when transitioning from the worst process parameters to the best process parameters. Similar results were obtained when performing the 3 point flexural test where an improvement in flexural stress at failure of 28.14% was achieved when the best process parameters are used (i.e., Batch A).

Measured values from the tensile and bending tests appearing in Table 5 are support the hypothesis described previously.

3.3. Microstructure results

Six CPLA parts were prepared for X-ray CT microstructural analysis which included three samples for each process parameter set found to produce the lowest and highest electrical resistances, as described in Section 2.3 to align with mechanical testing samples Batches A and B. The mean and standard deviation of void volume fraction percentage for these process parameter sets appear in Table 6, showing the reduction in void volume fraction when setting the best combination of printing parameters. Multiple views of the scans and void volume faction along the X- and Y-coordinate directions for the two process parameter sets are shown in Figs. 7 and 8. Note that the direction of extrusion in both scanned parts is identified as the Z-direction, while the Y-direction is normal to the print surface.

During the ironing process, the hot nozzle is passed over the last extruded layer to apply mechanical pressure in conjunction with heat to increase interlayer adhesion. The ironed part shown in Fig. 7(a) has a relatively rough surface compared to the non-ironed part in Fig 7 (b). Figs 7 (c) and (d) shows the 2D cross-section of the ironed and non-ironed parts respectively, where the gray area in the images is CPLA material and the black regions within the gray areas are voids. Results showed and average void volume fraction of 4.57% within the ironed part, while this amount is 5.68% in the non-ironed part. The contact pressure created during the ironing process for the parts shown in Fig 7 (c) and Figs 8 (a) and (b) decreases the size of the interlayer gaps, randomly distributes the remaining void content, and reduces the overall void volume fraction. This is contrasted in Fig 7(d) and Fig 8(a) and (b) for the non-ironed samples where relatively large interlayer voids primarily appear having triangular shapes within the microstructure.

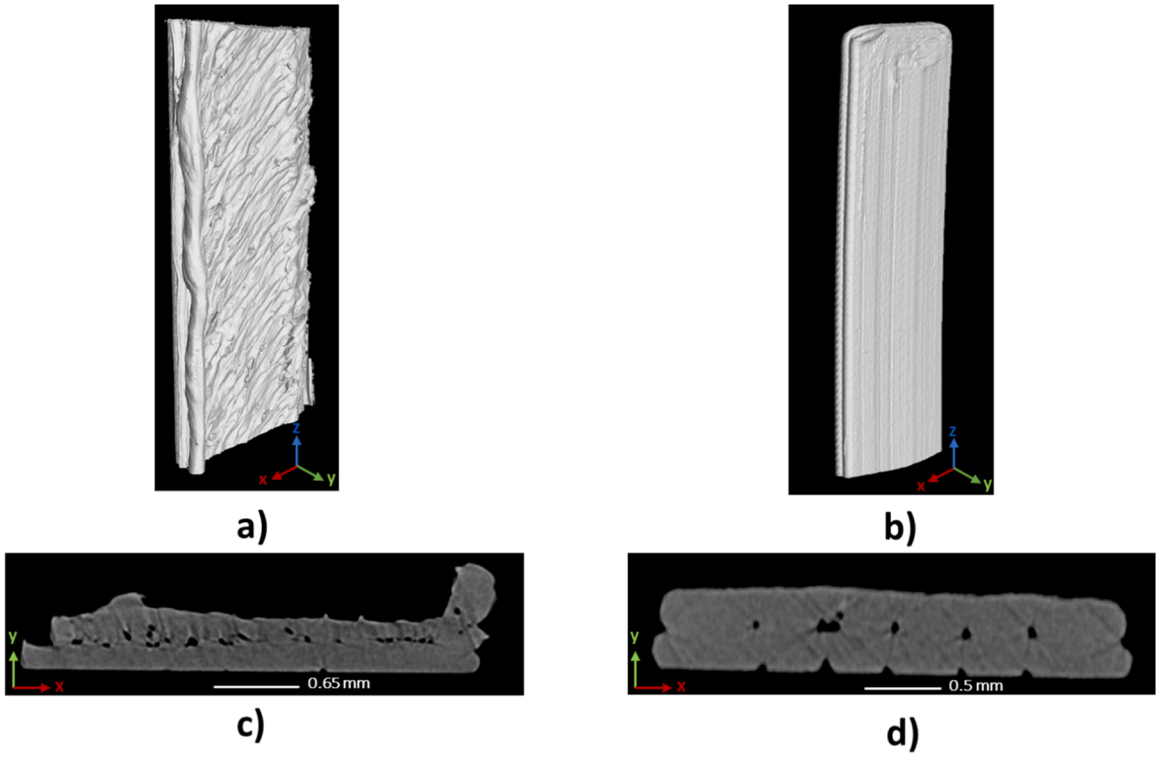

Fig. 7. CT images of CPLA a) 3D view of the ironed part b) 3D view of the non-ironed part c) 2D cross-section of the ironed part d) 2D cross-section of the non-ironed part

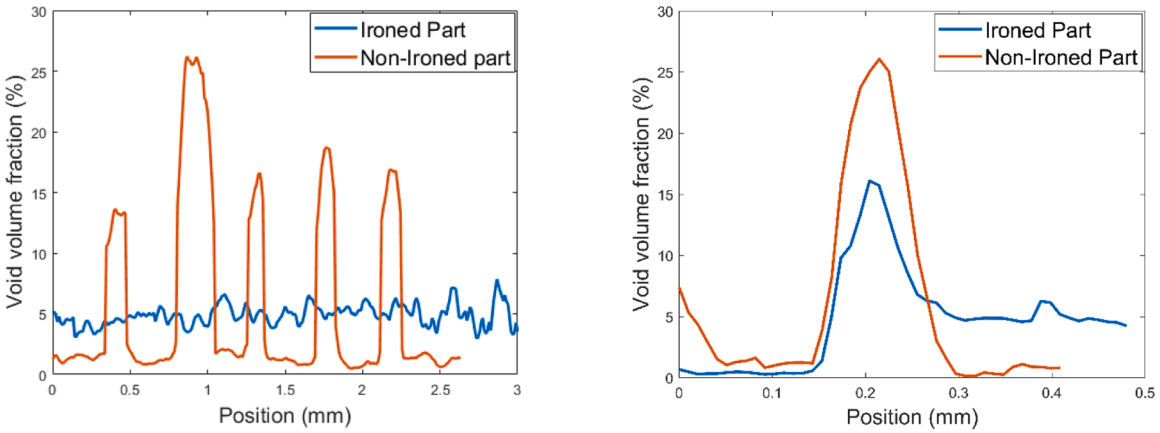

Fig. 8. Void volume fraction along the X- and Y-directions of CPLA : a) along the X-direction of ironed and non-ironed part b) along the Y-direction of ironed and non-ironed part

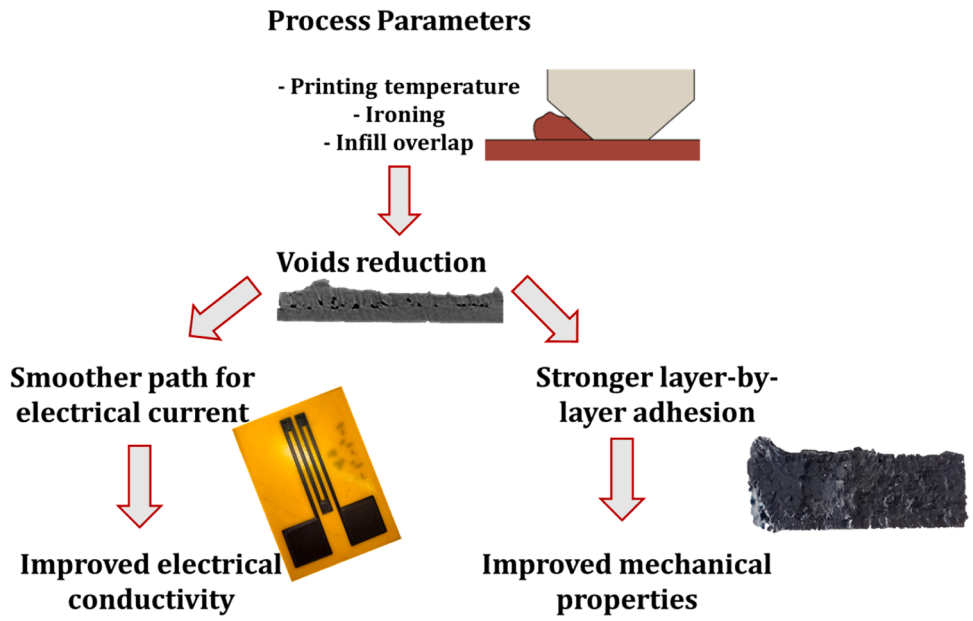

Fig. 9. Relationship among process parameters, microstructure, electrical properties and mechanical properties.

Table 7
Summary of Results

	Worst Parameter Set - B	Best Parameter Set - A	Improvement
Electrical Resistance	29.17 kΩ	15.12 kΩ	47.9 %
UTS	13.941 MPa	20.528 MPa	31.9 %
Tensile Strain at Failure	1.03	1.39	25.89 %
Flexural Stress at Failure	29.64 MPa	41.25 MPa	28.14%
Void Volume Fraction (%)	5.68	4.79	19.54%

3.4. Summary of Results

Results from Sections 3.1 to 3.3 show a clear relationship between process parameter selection, the microstructure of the fabricated components, and the resultant functional performance of CPLA sensors fabricated via MEX techniques, establishing the material-process-microstructure-function relationships for these sensors (see Fig. 9). Key findings that compare Batches A and B testing summarized in Table 7 yield the following observations:

- The selected process parameters (and in particular the ironing parameter) significantly increase the wetted area between consecutive layers, as shown in Fig 5(c), increasing the functional performance of CPLA sensors. This improvement in functional performance could also be attributed to an increase in the intermolecular diffusion and interlayer adhesion.
- The microstructure of CPLA is the key enabler to correlate electrical and mechanical properties, with the CT results clearly showing a direct correlation between these two properties. When the best process parameters (Table 4) are used, the whole 3D printed conductive structure is more compact, with a main void volume fraction of 4.57%. This void reduction led to an improvement in both performances. For the electrical performance, a reduced void content provides a smoother path to the electrical current to flow through, resulting in an increased conductivity (reduction of electrical resistance). In reference to the mechanical performance, as well-established in scientific literature, the reduced porosity produces a stronger layer-by-layer adhesion resulting in increased in mechanical properties.

4. Conclusions

In order for MEX to be used to produce functionally viable components, clear material-process-microstructure-function relationships must be established. In the present paper, a set of MEX process parameters, including ironing, nozzle temperature, and overlap, has been studied, taking advantage of the DoE approach, for the fabrication of CPLA sensors to minimize the final electrical resistance. The latter was improved 47.9 % when ironing, printing temperature and infill overlap parameters were set as ON, 250°C and 0.2 mm, respectively. The correlation among electrical properties, mechanical properties and microstructure was established where a significant improvement of electrical resistance (reduction of 47.9%), mechanical properties (UTS improvement of 31.9%; flexural strength improvement of 28.14%), and interlayer porosity (reduction of 19.54%) were realized. This works reduces the gap in knowledge on functional additive manufacturing of CPLA sensors which will advance MEX technology towards functional manufacturing.

CRediT authorship contribution statement

Gianni Stano: Conceptualization, Formal analysis, Methodology, Writing – original draft, Writing – review & editing. **Neshat Sayah:** Conceptualization, Formal analysis, Investigation, Methodology, Writing – original draft. **Douglas E. Smith:** Methodology, Writing – original draft. **Trevor J. Fleck:** Conceptualization, Formal analysis, Investigation, Methodology, Writing – original draft, Writing – review & editing.

Declaration of competing interest

The authors declare that they have no known competing financial interests or personal relationships that could have appeared to influence the work reported in this paper.

Data availability

Data will be made available on request.

Fundings

The authors would like to thank Baylor University for supporting this work.

References

[1] H. Liu, et al., 3D printed flexible strain sensors: from printing to devices and signals, Adv. Mater. 33 (8) (2021) 1–19, https://doi.org/10.1002/adma.202004782.
[2] M. Schouten, G. Wolterink, A. Dijkshoorn, D. Kosmas, S. Stramigioli, G. Krijnen, A review of extrusion-based 3D printing for the fabrication of electro- and biomechanical sensors, IEEE Sens. J. 21 (11) (2021) 12900–12912, https://doi.org/10.1109/JSEN.2020.3042436.
[3] A. Dijkshoorn, et al., Embedded sensing: integrating sensors in 3-D printed structures, J. Sensors Sens. Syst. 7 (1) (2018) 169–181, https://doi.org/10.5194/jsss-7-169-2018.
[4] A.M. Peterson, Review of acrylonitrile butadiene styrene in fused filament fabrication: a plastics engineering-focused perspective, Addit. Manuf. 27 (2019) 363–371, https://doi.org/10.1016/j.addma.2019.03.030. January.
[5] G. Stano, A. Di Nisio, A.M. Lanzolla, M.A. Ragolia, G. Percoco, Additive manufacturing for capacitive liquid level sensors, Int. J. Adv. Manuf. Technol. (2022), https://doi.org/10.1007/s00170-022-10344-7, 0123456789.
[6] K. Li, H. Wei, W. Liu, H. Meng, P. Zhang, C. Yan, 3D printed stretchable capacitive sensors for highly sensitive tactile and electrochemical sensing, Nanotechnology 29 (18) (2018), https://doi.org/10.1088/1361-6528/aaafa5.
[7] A.G. Samarentsis, G. Makris, S. Spinthaki, G. Christodoulakis, M. Tsiknakis, A. K. Pantazis, 3D-printed capacitive smart insole for plantar pressure monitoring, Phys. Sensors (2022) 1–18.
[8] L.Y.W. Loh, U. Gupta, Y. Wang, C.C. Foo, J. Zhu, W.F. Lu, 3D printed metamaterial capacitive sensing array for universal jamming gripper and human joint wearables, Adv. Eng. Mater. 23 (5) (2021) 1–9, https://doi.org/10.1002/adem.202001082.
[9] C.J. Hohimer, G. Petrossian, A. Ameli, C. Mo, P. Pötschke, 3D printed conductive thermoplastic polyurethane/carbon nanotube composites for capacitive and piezoresistive sensing in soft pneumatic actuators, Addit. Manuf. 34 (2019) 101281, https://doi.org/10.1016/j.addma.2020.101281. December2020.
[10] H.G. Kim, S. Hajra, D. Oh, N. Kim, H.J. Kim, Additive manufacturing of high-performance carbon-composites: an integrated multi-axis pressure and temperature monitoring sensor, Compos. Part B Eng. 222 (2021) 109079, https://doi.org/10.1016/j.compositesb.2021.109079 no. April, p.
[11] F. Grønborg, T.G. Zsurzsan, A.E. Daugaard, J. Spangenberg, D.B. Pedersen, Conductive compliant mechanisms: geometric tuning of 3D printed flexural sensors, Addit. Manuf. Lett. 3 (2022) 100088, https://doi.org/10.1016/j.addlet.2022.100088 no. August, p.
[12] O.F. Emon, F. Alkadi, M. Kiki, J.-W. Choi, Conformal 3D printing of a polymeric tactile sensor, Addit. Manuf. Lett. 2 (2021) 100027, https://doi.org/10.1016/j.addlet.2022.100027 no. December2022.
[13] M. Alsharari, B. Chen, W. Shu, Sacrificial 3D printing of highly porous, soft pressure sensors, Adv. Electron. Mater. 8 (1) (2022) 1–12, https://doi.org/10.1002/aelm.202100597.
[14] M. Arh, J. Slavič, Single-process 3D-printed triaxial accelerometer, Adv. Mater. Technol. 2101321 (2021) 1–7, https://doi.org/10.1002/admt.202101321.
[15] M. Arh, J. Slavič, M. Boltežar, Design principles for a single-process 3d-printed accelerometer – theory and experiment, Mech. Syst. Signal Process. 152 (2021), https://doi.org/10.1016/j.ymssp.2020.107475.
[16] M. Liu, Q. Zhang, Y. Zhao, Y. Shao, D. Zhang, Design and development of a fully printed accelerometer with a carbon paste-based strain gauge, Sensors (Switzerland) 20 (12) (2020) 1–17, https://doi.org/10.3390/s20123395.
[17] A. Dijkshoorn, M. Schouten, S. Stramigioli, G. Krijnen, Modelling of anisotropic electrical conduction in layered structures 3d-printed with fused deposition modelling, Sensors 21 (11) (2021) 1–37, https://doi.org/10.3390/s21113710.
[18] M. Arh, J. Slavič, M. Boltežar, Experimental identification of the dynamic piezoresistivity of fused-filament-fabricated structures, Addit. Manuf. 36 (2020) 101493, https://doi.org/10.1016/j.addma.2020.101493 no. April, p.
[19] A. Dijkshoorn, V. Ravi, P. Neuvel, S. Stramigioli, G. Krijnen, Mechanical interlocking for connecting electrical wires to flexible, FDM, 3D-printed conductors, in: FLEPS 2022 - IEEE Int. Conf. Flex. Printable Sensors Syst. Proc, 2022, pp. 27–30, https://doi.org/10.1109/FLEPS53764.2022.9781552.
[20] M.M. Mohammadi, et al., Additive manufacturing of recyclable, highly conductive, and structurally robust graphite structures, Addit. Manuf. Lett. 3 (2022) 100061, https://doi.org/10.1016/j.addlet.2022.100061 no. May, p.
[21] J.D. Banks, A. Emami, Carbon-based piezoresistive polymer nanocomposites by extrusion additive manufacturing: process, material design, and current progress, 3D Print. Addit. Manuf. (2022), https://doi.org/10.1089/3dp.2022.0153.
[22] N.A. Mohd Radzuan, A.B. Sulong, J. Sahari, A review of electrical conductivity models for conductive polymer composite, Int. J. Hydrogen Energy 42 (14) (2017) 9262–9273, https://doi.org/10.1016/j.ijhydene.2016.03.045.
[23] J.A. Cardenas, et al., Flash ablation metallization of conductive thermoplastics, Addit. Manuf. 36 (2020) 101409, https://doi.org/10.1016/j.addma.2020.101409 no. March, p.
[24] N. Lazarus, J.B. Tyler, J.A. Cardenas, B. Hanrahan, H. Tsang, S.S. Bedair, Direct electroless plating of conductive thermoplastics for selective metallization of 3D printed parts, Addit. Manuf. 55 (2022) 102793, https://doi.org/10.1016/j.addma.2022.102793 no. February, p.
[25] A.M. Stano, G. Di Nisio, A. Lanzolla, Fused filament fabrication of commercial conductive filaments : experimental study on the process parameters aimed at the minimization, repeatability and thermal characterization of electrical resistance, Int. J. Adv. Manuf. Technol. (111) (2020) 2971–2986, 2020.
[26] H. Watschke, K. Hilbig, T. Vietor, Design and characterization of electrically conductive structures additively manufactured by material extrusion, Appl. Sci. 9 (4) (2019) 1–25, https://doi.org/10.3390/app9040779.
[27] F. Daniel, A. Gleadall, A.D. Radadia, Influence of interface in electrical properties of 3D printed structures, Addit. Manuf. 46 (2021) 102206, https://doi.org/10.1016/j.addma.2021.102206 no. June, p.
[28] J. Zhang, B. Yang, F. Fu, F. You, X. Dong, M. Dai, Resistivity and its anisotropy characterization of 3D-printed acrylonitrile butadiene styrene copolymer (ABS)/carbon black (CB) composites, Appl. Sci. 7 (1) (2017), https://doi.org/10.3390/app7010020.
[29] K. Dembek, B. Podsiadły, M. Słoma, Influence of process parameters on the resistivity of 3D printed electrically conductive structures, Micromachines (Basel) 13 (8) (2022), https://doi.org/10.3390/mi13081203.
[30] T.B. Palmić, J. Slavič, M. Boltežar, Process parameters for FFF 3d-printed conductors for applications in sensors, Sensors (Switzerland) 20 (16) (2020) 1–21, https://doi.org/10.3390/s20164542.
[31] Y. Tao, et al., A review on voids of 3D printed parts by fused filament fabrication, J. Mater. Res. Technol. 15 (2021) 4860–4879, https://doi.org/10.1016/j.jmrt.2021.10.108.
[32] A.C. Abbott, G.P. Tandon, R.L. Bradford, H. Koerner, J.W. Baur, Process-structure-property effects on ABS bond strength in fused filament fabrication, Addit. Manuf. 19 (2018) 29–38, https://doi.org/10.1016/j.addma.2017.11.002.
[33] J. Butt, R. Bhaskar, V. Mohaghegh, Investigating the effects of ironing parameters on the dimensional accuracy, surface roughness, and hardness of FFF-printed thermoplastics, J. Compos. Sci. 6 (5) (2022), https://doi.org/10.3390/jcs6050121.
[34] M. Caputo, O. Rashwan, D. Waryoba, K. McDade, Surface texture and thermo-mechanical properties of material extruded and ironed polylactic acid, Addit. Manuf. 59 (2022) 103084, https://doi.org/10.1016/j.addma.2022.103084 no. PA, p.

[35] M. Sardinha, C.M.S. Vicente, N. Frutuoso, M. Leite, R. Ribeiro, L. Reis, Effect of the ironing process on ABS parts produced by FDM, Mater. Des. Process. Commun. 3 (2) (2021) 1–7, https://doi.org/10.1002/mdp2.151.
[36] N. Aliheidari, R. Tripuraneni, A. Ameli, S. Nadimpalli, Fracture resistance measurement of fused deposition modeling 3D printed polymers, Polym. Test. 60 (2017) 94–101, https://doi.org/10.1016/j.polymertesting.2017.03.016.
[37] R. Côté, V. Demers, N.R. Demarquette, S. Charlon, J. Soulestin, A strategy to eliminate interbead defects and improve dimensional accuracy in material extrusion 3D printing of highly filled polymer, Addit. Manuf. 68 (2023) 1–11, https://doi.org/10.1016/j.addma.2023.103509, no. February, pp.
[38] N. Sayah, D.E. Smith, Effect of process parameters on void distribution, volume fraction, and sphericity within the bead microstructure of large-area additive manufacturing polymer composites, Polymers. (Basel) 14 (23) (2022), https://doi.org/10.3390/polym14235107.
[39] R.P. Wool, K.M. O'Connor, A theory crack healing in polymers, J. Appl. Phys. 52 (1998) 5953–5963, no. June1981.
[40] T.J. Coogan, D.O. Kazmer, Healing simulation for bond strength prediction of FDM, Rapid Prototyp. J. 23 (3) (2017) 551–561, https://doi.org/10.1108/RPJ-03-2016-0051.
[41] T.J. Coogan, D.O. Kazmer, Prediction of interlayer strength in material extrusion additive manufacturing, Addit. Manuf. 35 (2020) 101368, https://doi.org/10.1016/j.addma.2020.101368 no. June, p.
[42] A. Dey, N. Yodo, A systematic survey of FDM process parameter optimization and their influence on part characteristics, J. Manuf. Mater. Process. 3 (3) (2019) 64, https://doi.org/10.3390/jmmp3030064.